

Photoionization of helium with ultrashort XUV laser pulses

I.F. Barna and J.M. Rost^a

Max-Planck-Institute for the Physics of Complex Systems, Nöthnitzer Straße 38, 01187 Dresden, Germany

Received: 8 April 2003

Published online 9 September 2003 – © EDP Sciences, Società Italiana di Fisica, Springer-Verlag 2003

Abstract. Coupled-channel calculations for multiphoton ionization probabilities of helium through interaction with intensive short laser pulses are presented. Besides Slater-like orbitals we use regular Coulomb wavepackets in our configurational interaction basis to describe the continuum. Linearly polarized laser pulses of 3.8 fs duration and $2.96 \times 10^{14} \text{ Wcm}^{-2}$ peak intensity have been used for frequencies between 0.2–1.2 a.u. The results are compared with other *ab initio* calculations.

PACS. 32.80.Fb Photoionization of atoms and ions – 32.80.Wr Other multiphoton processes

1 Introduction

Photoionization of the helium atom in an intense laser field has been extensively studied both, experimentally and theoretically [1–5]. The first non-perturbative fully correlated three-dimensional calculations have been performed in the frame work of *R*-matrix Floquet (RMF) theory to describe multiphoton processes [6]. Later, explicitly time-dependent configuration interaction approaches have been used for the interaction with ultra short laser pulses [7, 8], where in [7] time-dependent restricted Hartree-Fock calculations were also presented. A mixed finite-difference basis set technique was employed in [9] to calculate the double-ionization probabilities for pulses. Finally, the intense-field many-body *S*-matrix theory (IMST) has been developed to calculate single- and multiple-ionization of noble gases [10]. Further details including references and an overview over various methods are given in the review by Lambropoulos *et al.* [11].

Here, we report on the new implementation of our coupled-channel method for laser driven atomic processes. So far, the method has been successfully applied for heavy ion helium collisions to calculate total cross-sections [12, 13]. We take the electron-electron interaction fully into consideration which is important for double-ionization. To represent bound states and resonances we use Slater-type orbitals. A special feature in our explicitly correlated basis are regular Coulomb wavepackets which we use to discretize the continua. As we will show, the low lying single- and double Coulomb continua can be approximated well for dynamics in short XUV pulses with the help of these wavepackets. Alternatively, this is done by numerically calculating single-electron wave functions in a finite box [14]. To identify the double excited states embedded in the single electron continuum (*e.g.* $2s2s$) we

adopted the method of complex scaling [15]. Atomic units are used otherwise mentioned.

2 Theory

To describe the ionization process in the laser pulse we solve the time-dependent Schrödinger equation

$$i \frac{\partial}{\partial t} \Psi(\mathbf{r}_1, \mathbf{r}_2, t) = \left(\hat{H}_{\text{He}} + \hat{V}(t) \right) \Psi(\mathbf{r}_1, \mathbf{r}_2, t), \quad (1)$$

where \hat{H}_{He} is the Hamiltonian of the unperturbed spin-independent helium atom

$$\hat{H}_{\text{He}} = \frac{\mathbf{p}_1^2}{2} + \frac{\mathbf{p}_2^2}{2} - \frac{2}{r_1} - \frac{2}{r_2} + \frac{1}{|\mathbf{r}_1 - \mathbf{r}_2|}. \quad (2)$$

$\hat{V}(t)$ is the interaction operator between the laser pulse and the atomic electrons which will be specified later. To solve (1) we expand $\Psi(\mathbf{r}_1, \mathbf{r}_2, t)$ in the basis $\{\Phi_j\}$ of eigenfunctions of the time independent Schrödinger equation

$$\hat{H}_{\text{He}} \Phi_j = E_j \Phi_j \quad (3)$$

to yield

$$\Psi(\mathbf{r}_1, \mathbf{r}_2, t) = \sum_{j=1}^N a_j(t) \Phi_j(\mathbf{r}_1, \mathbf{r}_2) e^{-iE_j t}, \quad (4)$$

where the $a_j(t)$ are the time-dependent expansion coefficients and E_j are the eigenvalues in (3). Inserting (4) the time-dependent Schrödinger equation (1) leads to a system of first-order differential equations for the expansion coefficients

$$\frac{da_k(t)}{dt} = -i \sum_{j=1}^N V_{kj} e^{i(E_k - E_j)t} a_j(t) \quad (k = 1, \dots, N) \quad (5)$$

^a e-mail: rost@mpipks-dresden.mpg.de

with the coupling matrix elements

$$V_{kj} = \langle \Phi_k | \hat{V} | \Phi_j \rangle. \quad (6)$$

Denoting the ground state with channel $j = 1$, the initial condition before the laser pulse is applied reads

$$a_j(t \rightarrow -\infty) = \begin{cases} 1 & j = 1 \\ 0 & j \neq 1. \end{cases} \quad (7)$$

The probabilities for transitions into final helium states j after the pulse are simply given by

$$P_j = |a_j(t \rightarrow +\infty)|. \quad (8)$$

For the ionization probability one must sum the P_j which correspond to the discretized channels formed by the wavepackets solved numerically.

The eigenfunctions Φ_j in (3) are obtained by diagonalizing the Hamiltonian in a basis of orthogonal symmetrized two-particle functions f_μ so that

$$\Phi_j(\mathbf{r}_1, \mathbf{r}_2) = \sum_{\mu} b_{\mu}^{[j]} f_{\mu}(\mathbf{r}_1, \mathbf{r}_2). \quad (9)$$

In the following we restrict ourselves to singlet helium states only. For the single-particle wave functions we use an angular momentum representation with spherical harmonics $Y_{l,m}$, hydrogen-like radial Slater functions and radial regular Coulomb wavepackets. The Slater function reads

$$S_{n,l,m,\kappa}(\mathbf{r}) = c(n, \kappa) r^{n-1} e^{-\kappa r} Y_{l,m}(\theta, \varphi), \quad (10)$$

where $c(n, \kappa)$ is the normalization constant. A regular Coulomb wavepacket

$$C_{k,l,m,Z}(\mathbf{r}) = q(k, \Delta k) Y_{l,m}(\theta, \varphi) \int_{E_k - \Delta E_k/2}^{E_k + \Delta E_k/2} F_{k,l,Z}(r) dk \quad (11)$$

with normalization constant $q(k, \Delta k)$ is constructed from radial Coulomb function of the well-known form [16]

$$F_{k,l,Z}(r) = \sqrt{\frac{2k}{\pi}} e^{\frac{\pi\eta}{2}} \frac{(2\rho)^l}{(2l+1)!} e^{-i\rho} |\Gamma(l+1-i\eta)| \times {}_1F_1(1+l+i\eta, 2l+2, 2i\rho), \quad (12)$$

where $\eta = Z/k$, $\rho = kr$.

The wavepackets cover a small energy interval ΔE_k and thereby form a discrete representation of the continuum which can be incorporated into our finite basis set. The normalized Coulomb wavepackets are calculated up to 315 a.u. radial distance or more to achieve a deviation of less than one percent from unity in their norm. With the help of the Coulomb wavepackets we can make calculations for quiver radii ($r_q = \sqrt{I/\omega^2}$) of more than 50 a.u. (I stands for the pulse intensity and ω for the photon energy). This would be hardly possible with bound wave functions only.

Table 1. Some energy levels of bound singly and doubly excited states used in our calculations, compared with ^abasis set calculations from [17], ^bCI calculation results [7] and ^ccomplex-coordinate rotation calculations from [18].

states	our results	other theory
1s1s	-2.9011	-2.9037 ^a
1s2s	-2.1441	-2.1460 ^a
1s3s	-2.0607	-2.0612 ^a
1s4s	-2.0333	-2.0335 ^a
2s2s	-0.7297	-0.7779 ^a
2s3s	-0.5711	-0.5899 ^a
2s4s	-0.5372	-0.5449 ^a
2s5s	-0.5133	-0.5267 ^a
1s2p	-2.1233	-2.1238 ^b
1s3p	-2.0550	-2.0551 ^b
1s4p	-2.0309	-2.0310 ^b
2s2p	-0.6472	-0.6931 ^c
2s3p	-0.5821	-0.5971 ^c
2s4p	-0.5451	-0.5640 ^c
2s5p	-0.5335	-0.5470 ^c
3s3p	-0.2998	-0.3356 ^c
1s3d	-2.0556	-2.0556 ^b
1s4d	-2.0312	-2.0313 ^b
2s3d	-0.5497	-0.5692 ^c
2s4d	-0.5295	-0.5564 ^c

In our approach two different effective charges Z have been used to take into account the difference between the singly and the doubly ionized electrons. For singly ionized states we have used $Z = 1.0$, and $Z = 2.0$ for the doubly ionized case. A slight deviation from the effective charge gives practically no change in the final spectrum. We cover the single- and double-continuum up to 6 a.u. energy equidistantly.

Out of the single particle states (5) we have used 17 s -functions (9 Slater functions (sf), 4 wavepackets (wp) with $Z = 1.0$ and 4 wp with $Z = 2.0$), 18 p -functions (6 sf, 6 wp with $Z = 1.0$ and 6 wp with $Z = 2.0$) and 12 d -functions (4 sf, 4 wp with $Z = 1.0$ and 4 wp $Z = 2.0$) to construct the symmetrized basis functions $f_{\mu}^{LM}(\mathbf{r}_1, \mathbf{r}_2)$. For the $L = 0$ configurations we have used $ss + pp + dd$ angular correlated wave functions to get a ground state energy of -2.901 a.u. which is reasonably accurate compared to the “exact” value of -2.903 a.u. For the $L = 1, 2$ states we have used only sp or sd configurations.

To test the convergence of our basis we have used all the 465 basis states at first, up to 27 a.u. energy. Our results clearly demonstrate that the channels above 3 a.u. contribute very little to the ionization probabilities. The low lying singly and doubly excited states used in our calculations are listed in Table 1.

Between the first ionization threshold (-2.0 a.u.) and the lowest autoionizing bound state (-0.6931 a.u. for $L = 1$) our basis contains 22 states providing the major

contribution for single ionization. Below the double-ionization threshold (0.0 a.u.) autoionizing bound states (such as $2s^2$) are embedded in the low lying single-electron continuum. Our basis describes the lowest 11 autoionized listed in Table 1. These resonances are important to describe ionization quantitatively.

We restrict ourselves to linearly polarized laser pulses whose coupling to the atomic electrons we describe in the length gauge and in dipole approximation,

$$\hat{V}(t) = - \sum_{i=1,2} \mathbf{E}(t) \cdot \mathbf{r}_i, \quad (13)$$

where the electric field is defined through the vector potential

$$\mathbf{E}(t) = - \frac{\partial}{\partial t} \mathbf{A}(t). \quad (14)$$

The velocity gauge was used for convergence test calculations only. At laser intensities larger than $2 \times 10^{14} \text{ Wcm}^{-2}$ we can verify the calculations of [7], the deviation between the two gauges is less than a factor of two.

The laser pulse we use is polarized along the z -axis and has a \sin^2 envelope,

$$\mathbf{A}(t) = A_0 \left(\sin \frac{\pi t}{T} \right)^2 \sin(\omega t) \mathbf{e}_z. \quad (15)$$

3 Results and discussion

Having solved the time-independent Schrödinger equation as described we get the ionization probabilities by numerically solving for the coefficients $a_j(t)$ from (5) in time. To this end the coupling matrix (6) is calculated at 820 different points in time and interpolated with a quadratic spline first. Then the coupled-channel equations (5) are solved numerically by using a Runge-Kutta-Fehlberg method of order five, embedding a fourth-order automatic time step regulation algorithm. The pulse duration is kept constant at 3.8 fs (158.3 a.u.) and the peak intensity at $2.96 \times 10^{14} \text{ Wcm}^{-2}$ (0.0084 a.u.) as well.

We compare our results for ionization in Figure 1 with the calculations of [7,8] for a range of photon energies. Overall the agreement with the two other calculations is good. A more detailed look at high photon energies reveals that around and above the single photon ionization threshold (0.9 a.u.) all three results are in good agreement. At $\omega \approx 0.78$ a.u. the *resonant* one photon $1s \rightarrow 2p$ excitation takes place. This facilitates a two-photon absorption which takes the electron into the single electron continuum at $E = -1.343$ a.u. If the numerical representation has not enough states in this region the corresponding calculations underestimate the ionization probability which explains the dip in the results of [7]. Our results are much better at this energies. but still a factor of 1.5 lower than the involved calculation of [8].

At small photon energies between 0.2–0.3 a.u. all three calculations differ from each other indicating the different representations of the electron continuum. In general, small photon energy means that more photons must be

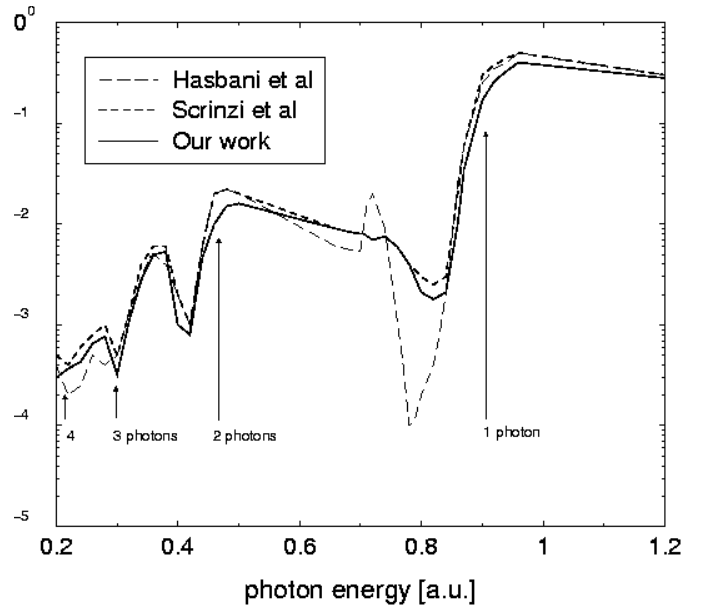


Fig. 1. Ionization probabilities of the helium atom with a \sin^2 -shaped pulse of 3.8 fs duration and peak intensity $2.97 \times 10^{14} \text{ Wcm}^{-2}$. The dashed line is the work of [7], the short dashed line shows the results obtained in [8] and the solid line represent our calculations. The arrows indicate the different photon ionization thresholds.

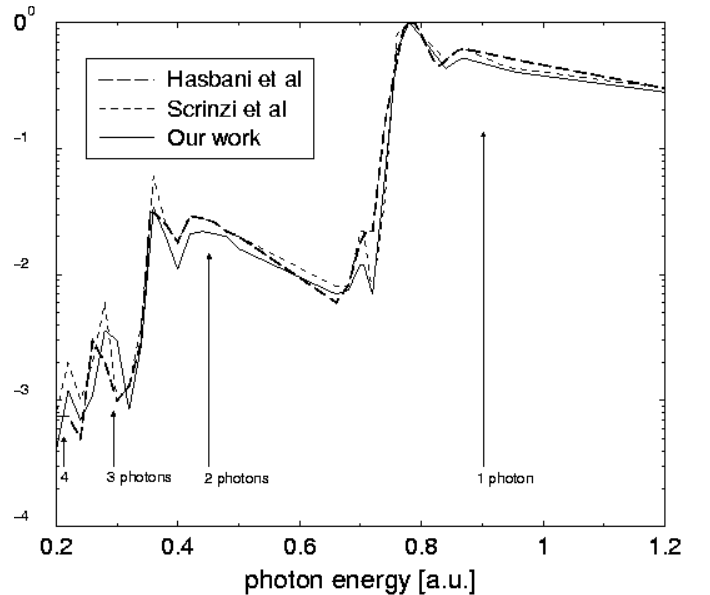


Fig. 2. Ionization and excitation probabilities of the helium. Notation is the same as in Figure 1.

absorbed for ionization and a higher density of states in the continuum is required. As a rule of thumb the inverse of the density of states must be smaller than the bandwidth of the laser, here about $\Delta\omega \approx 0.1$.

Figure 2 shows a comparison for ionization plus excitation. The parameters of the pulse and the basis used is the same as before. The three different calculations show good agreement again. Differences at low energies have the

same reason as explained for ionization. One can see the Rabi-like oscillations at $\omega = 0.72$ photon energy. At the resonant one photon $1s1s \rightarrow 1s2p$ transition ($\omega = 0.78$) the excitation probability is close to unity. Above this resonance frequency all the three calculations show a slowly decreasing behaviour. At photon energies between 0.3–0.36 a.u. and 0.5–0.64 a.u. no significant excitation can occur due to a lack of excited states which can be populated. Therefore, Figures 1 and 2 show the same (ionization) probabilities.

4 Summary and outlook

We have presented coupled-channel calculations for ionization and excitation of helium in ultra short laser pulses. Linearly polarized laser pulses were applied in the length gauge. The velocity gauge was used to check the convergence only. As pulse shape we used \sin^2 -function with duration of 3.8 fs and peak intensity of $2.96 \times 10^{14} \text{ Wcm}^{-2}$ for photon energy $0.2 \leq \omega \leq 1.2$. The channel functions were built up by Slater functions mainly to describe the bound state and regular Coulomb wavepackets to approximate the continua. The accuracy we achieve lies in between the elaborate calculations by [8] and the simpler calculations by [7]. Therefore, in combination with the speed of the code, the method described appears to be suitable to simulate optimal control with genetic codes which we plan for the future.

References

1. X.F. Li, A. L’Huillier, M. Ferray, L.A. Lompré, G. Mainfray, Phys. Rev. A **39**, 5751 (1989)
2. E. Mevel, P. Breger, R. Trainham, G. Petite, P. Agostini, Phys. Rev. Lett. **70**, 406 (1993)
3. K. Kondo, A. Sagisaka, T. Tamida, Y. Nabekawa, S. Watanabe, Phys. Rev. A **48**, R2531 (1993)
4. B. Walker, B. Sheehy, L.F. DiMauro, P. Agostini, K.J. Schafer, K.C. Kulander, Phys. Rev. Lett. **73**, 1227 (1994)
5. K. Miyazaki, H. Takada, Phys. Rev. A **52**, 3007 (1995)
6. P.G. Burke, P. Francken, C.J. Joachain, Europhys. Lett. **13**, 617 (1990); J. Phys. B: At. Mol. Opt. Phys. **25**, 2809 (1992)
7. R. Hasbani, E. Cormier, H. Bachau, J. Phys. B: At. Mol. Opt. Phys. **33**, 2101 (2000)
8. A. Scrinzi, B. Piraux, Phys. Rev. A **58**, 1310 (1998)
9. D. Dundas, K.T. Taylor, J.S. Parker, E.S.J. Smyth, Phys. B: At. Mol. Opt. Phys. **32**, L231 (1999)
10. F.H.M. Faisal, A. Becker, in *Selected Topics on Electron Physics*, edited by D.M. Campbell, H. Kleinoppen (Plenum, New York, 1996), p. 317
11. P. Lambropoulos, P. Maragakis, J. Zhang, Phys. Rep. **305**, 203 (1998)
12. I.F. Barna, N. Grün, W. Scheid, Eur. Phys. J. D **25**, 239 (2003)
13. I.F. Barna, *Ionization of helium in relativistic heavy-ion collisions*, Doctoral thesis, University Giessen (2002), “Giessener Elektronische Bibliothek” <http://geb.uni-giessen.de/geb/volltexte/2003/1036>
14. J. Zhang, P. Lambropoulos, J. Phys. B: At. Mol. Opt. Phys. **28**, L101 (1995)
15. N. Moiseyev, Phys. Rep. **302**, 211 (1998)
16. M. Abramowitz, A. Stegun, *Handbook of Mathematical Functions* (Dover Publications Inc., New York, 1972)
17. A. Bürgers, D. Wintgen, J.M. Rost. J. Phys. B: At. Mol. Opt. Phys. **28**, 3163 (1995)
18. Y.K. Ho, Phys. Rev. A **34**, 4402 (1986); Z. Phys. D **21**, 191 (1991); Y.K. Ho, A.K. Bhatia, Phys. Rev. A **44**, 2895 (1991)